Nanoscale

PAPER

View Article Online
View Journal | View Issue

Cite this: *Nanoscale*, 2023, **15**, 14061

Probing antiferromagnetism in exfoliated Fe_3GeTe_2 using magneto-transport measurements†

Stasiu T. Chyczewski, *[a] Ji Shi,[a] Hanwool Lee,[a] Paolo F. Furlanetto,[b] Kai Xu,[a] Arend M. van der Zande[b] and Wenjuan Zhu *[a]

Received 5th March 2023,
Accepted 2nd August 2023

DOI: 10.1039/d3nr01022h

rsc.li/nanoscale

Among the material class of van der Waals magnets, Fe_3GeTe_2 (FGT) has emerged as one of the most studied owing to features such as its relatively high Curie temperature, metallic nature, and large spin polarization. Though most studies only investigate its explicitly ferromagnetic properties, FGT is also predicted to have an antiferromagnetic phase in the out-of-plane direction emerging at temperatures below 150 K, leading to a blend of ferromagnetic and antiferromagnetic ordering. Here, we explore the emergence of this phase and its effects in FGT/h-BN heterostructures using magneto-transport measurements. The devices' anomalous Hall and magnetoresistance responses exhibit a complex trend with temperature that is consistent with multiple magnetic phases. In addition to the usual out-of-plane sensing, we also rotate the applied field to the in-plane direction and observe behavior resembling the planar topological Hall effect. Intriguingly, this response follows a similar temperature trend to the out-of-plane response. We also use the out-of-plane anomalous Hall response to show that, at sufficiently low temperatures, both positive and negative field-cooling results in an increased saturation Hall resistance. Such a field-cooling divergence is consistent with antiferromagnetic ordering resulting in a spin-glass like state in the sample. In addition to providing insight into one of the most exciting candidate materials for 2D magnetic devices, our work demonstrates the power of magneto-transport measurements to probe complex behavior in vdW magnets where common magnetometry techniques used on bulk samples may not be viable.

Introduction

Since their discovery, vdW magnets have attracted large amounts of interest in the world of condensed matter physics. Their unique properties such as high spin polarizations, large anomalous Hall angles, and potential for atomically sharp heterostructures make them exciting candidates for spintronic devices.[1–3] Their low dimensionality also provides an opportunity to study novel physical phenomena such as magnetic skyrmions.[4,5] Among the most common vdW magnets studied is Fe_3GeTe_2 (FGT). Compared to other early 2D magnets like CrI_3 and $Cr_2Ge_2Te_6$ (both of which are semiconducting), FGT exhibits metallic behavior and a high Curie temperature typically reported as 220 K at bulk.[6–9] FGT's relative ease of use has led to its incorporation in many studies of layered magnets. FGT has, for example, been used to create all-2D magnetic tunnel junctions (MTJs) and showed a remarkably high spin polarization of up to 0.66 at sufficiently low temperature.[10] FGT has also been used to demonstrate the electrical control of magnetism *via* both gating and spin orbit torques (SOT), pre-requisites for advanced magnetic devices.[11–13]

Despite the wealth of studies on the material, there is limited work focusing on the complex magnetic phases that have been shown to emerge. Particularly, the coexistence of ferro/anti-ferromagnetism in FGT is seldom discussed. As competing magnetic phases can significantly affect device properties (*e.g.*, result in spin-glass like behavior), understanding them is critical to device design. For FGT, antiferromagnetism is sometimes discussed in the context of the oxide that forms on the material. Like many other ferromagnets, FGT forms a native antiferromagnetic oxide that can cause exchange bias (EB).[14–16] This effect can be particularly strong in FGT due to its layered nature and rapid oxidation. Aside from interfacial effects like exchange bias, FGT is also predicted to exhibit antiferromagnetic behavior intrinsically without an oxide layer. Past experiments on bulk FGT crystals have shown the emergence of a competing antiferromagnetic phase at 150 K, with the ferromagnetic component becoming suppressed at low

[a]*Department of Electrical and Computer Engineering, University of Illinois at Urbana-Champaign, Urbana, Illinois 61801, USA. E-mail: stasiuc2@illinois.edu, wjzhu@illinois.edu*
[b]*Department of Mechanical Science and Engineering, University of Illinois at Urbana-Champaign, Urbana, Illinois 61801, USA*
† Electronic supplementary information (ESI) available. See DOI: https://doi.org/10.1039/d3nr01022h

temperature.[17] FGT's metallic nature provides a convenient means to study this behavior using electrical transport as opposed to far more complex micro-magnetometry techniques like nitrogen vacancy magnetometry.[18] Specifically, the anomalous Hall effect (AHE) and longitudinal magnetoresistance (MR) can give insight into the material's magnetic ordering.

In this work, we use magneto-transport measurements to probe the presence of antiferromagnetic behavior in iron-enriched FGT. We observed a non-monotonic trend in the anomalous Hall effect (AHE) and longitudinal magnetoresistance signal strength with temperature, a planar topological Hall effect, and a field-cooling (FC) divergence in FGT. Each of these phenomena suggests complex magnetic phases in the material consistent with a blend of ferromagnetic and antiferromagnetic behavior.

Experimental

We prepared devices using exfoliated Fe_3GeTe_2 crystals purchased from 2D Semiconductors. The crystals were exfoliated using the Scotch tape method in a <20 ppm O_2 nitrogen glovebox onto an Si/SiO_2 wafer to prevent significant oxidation of the flakes. The exfoliated flakes were then transferred onto pre-patterned Ti/Au electrodes using polycarbonate-coated polydimethylsiloxane (PDMS) lenses on glass transfer slides (see Fig. S1† for more details).[19] The transfer process is then repeated with a hexagonal boron nitride (h-BN) flake to cover the FGT, protecting it from air and allowing it to be removed from the glovebox without immediate risk of damage. During the process, the exfoliated flake is never exposed to the atmosphere. Such care is necessary as even momentary exposure to air can alter device properties.[11–14] Upon removal, we measured devices immediately as while h-BN capping slows degradation, it does not completely prevent it and changes in sample behavior arise over long periods of time. Studied FGT flakes have thicknesses in the range of 30 nm to 260 nm (see Fig. S2† for examples). The thickness of most flakes used in this study brings their magnetic properties close to that of bulk FGT.[6] We completed all magneto-transport measurements using the AC ETO option of a Quantum Design Physical Property Measurement System (PPMS) cryostat.

Results and discussion

FGT's unit cell exhibits hexagonal symmetry and is a member of the $P6_3/mmc$ space group.[9] Individual vdW layers are about 0.8 nm thick and consist of iron and germanium atoms sandwiched in between two layers of tellurium atoms. This relatively thick vdW layer allows for more intralayer exchange interactions to occur between magnetic ions, stabilizing the magnetic ordering at higher temperatures compared to many other vdW magnets. Other stoichiometries of FGT (*e.g.*, Fe_4GeTe_2 and Fe_5GeTe_2) have higher Curie temperatures than Fe_3GeTe_2 for the same reason.[20] Energy dispersive X-ray spectroscopy (EDS) measurements on our crystals show a higher iron content than expected, with the measured atomic ratios of Fe : Ge : Te being approximately 4.5 : 1 : 1.8, suggesting iron doping in the sample, as depicted in Fig. S3.† Schematics for a typical device made with our methods are shown in Fig. 1a and b, with an optical image of a real device shown in Fig. 1c. This device's FGT is estimated to be 120 nm thick based on transport measurements. A standard Hall sensing geometry is used. Flakes used in all devices are irregularly shaped as they cannot be etched without exposing them to the atmosphere. As a result, small offsets are usually present in the Hall signals due to asymmetries in the contacts. These do not significantly affect the signal and are removed by subtracting the average from the measurements. Standard four-point resistance measurements on flakes indicate that the FGT flake is metallic, as indicated by the device's low longitudinal resistance (R_{xx}) and its monotonic decrease with decreasing temperature as shown in Fig. 1d. Additionally, the devices did not exhibit any gate modulation when the substrate was used as a backgate, which further confirmed the metallic nature of FGT.

We first measure the temperature dependence of magnetic behavior in FGT samples with a magnetic field parallel to the out-of-plane direction using the AHE. In a magnetic conductor, the Hall resistance caused by an out-of-plane magnetic field can usually be expressed as $R_{xy} = R_0H_Z + R_sM_z$, where H_z is the applied perpendicular magnetic field, M_z is the perpendicular magnetization, and R_0 and R_s are the ordinary and anomalous Hall coefficients, respectively.[21] As FGT is a metallic ferromagnet, the normal Hall resistance is negligible compared with the anomalous Hall resistance in the magnetic field range of interest (*i.e.*, $R_0H_Z \ll R_sM_z$). As a result, the measured Hall resistance can be treated as being directly proportional to the sample magnetization. The applied magnetic field was swept from −2 to +2 Tesla at temperatures starting from 300 K down to 5 K. Measured AHE hysteresis loops at select temperatures are shown in Fig. 2a. Compared to other reports of Fe_3GeTe_2, our sample's AHE response persists even up to room temperature, which we attribute to the high iron content in the material. At temperatures above 220 K the response resembles that of a super-paramagnetic material, with non-linearity but no hysteresis discernable. Similar to previous studies, however, the hysteresis window begins to open and a remanence appears at 220 K. The relatively narrow hysteresis in our samples suggests that the anisotropy axis may not lie completely in the out of plane direction and is instead canted with respect to the sample vertical. For the devices with thinner FGT flakes (*e.g.*, 30 nm), the hysteresis widens (see Fig. S4†) and the coercivity increases, consistent with previous reports.[9,22,23] This behavior indicates increasing perpendicular magnetic anisotropy (PMA) as the thickness decreases. Notably, the derivative of the Hall resistance ($dR_{xy}/d(\mu_0H)$) follows a non-monotonic trend with temperature as shown in the inset of Fig. 2a. The $dR_{xy}/d(\mu_0H)$ increases with decreasing temperature until a peak at around 120 K before decreasing. This behavior is consistently observed in FGT samples fabricated with our crystals. This contrasts quite sharply with the usual monotonic change in magnetic behavior (*e.g.*, suscepti-

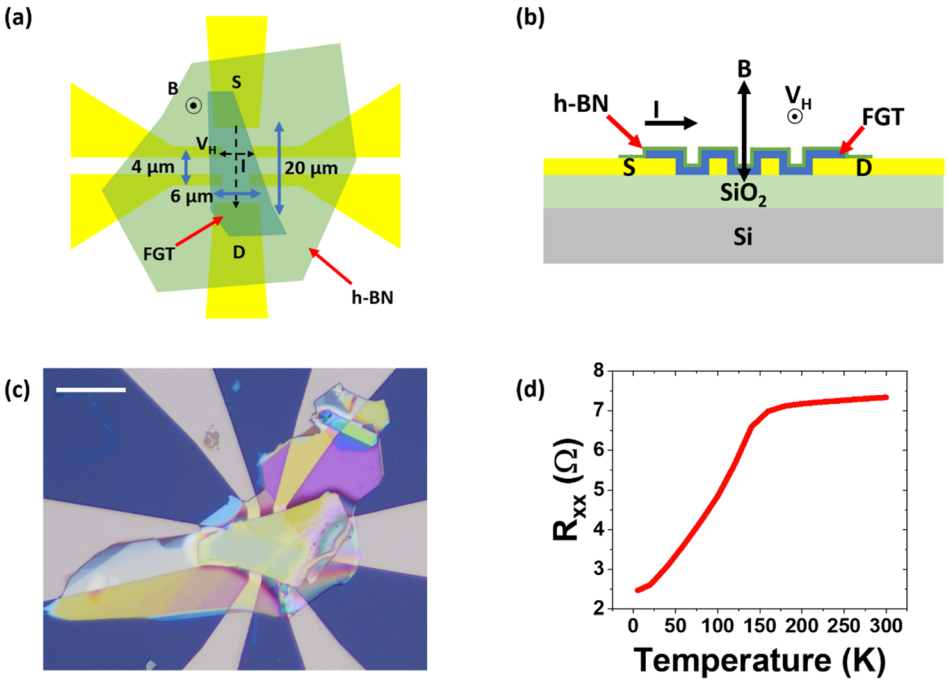

Fig. 1 Typical fabricated FGT device. (a) Top-view schematic showing flake placement and sensing geometry. (b) Side-view schematic showing flake placement and sensing geometry. (c) Optical image of a covered FGT device made using our methods. Subsequent magneto-transport measurements presented in the main text were all taken from this specific device. Scale bar: 20 μm. (d). Longitudinal four-point resistance *vs.* temperature measurement for an FGT device, demonstrating metallic nature.

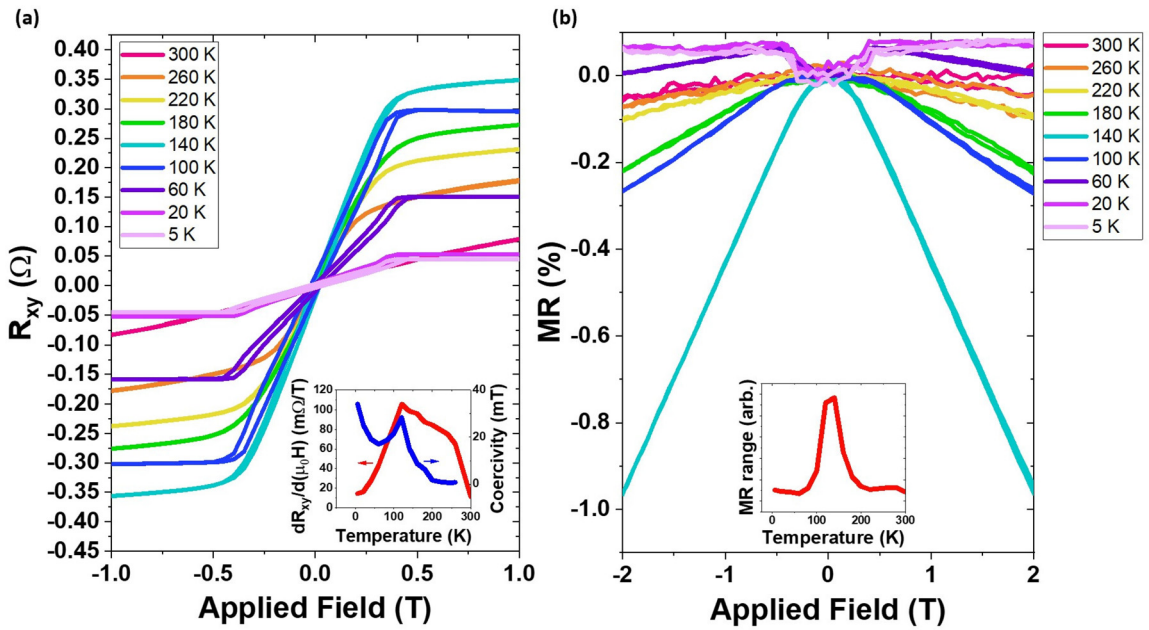

Fig. 2 Basic Hall and magnetoresistance responses. (a) Hall response of standard FGT from +1 to −1 T at various temperatures, showing narrow hysteresis. Inset: $dR_{xy}/d(\mu_0 H)$ and coercivity *vs.* temperature. See Fig. S5 for sweeps at additional temperatures and Fig. S4a–c† for sweeps from other devices. (b) Two-point magnetoresistance sweeps at various temperatures. Inset: maximum range of MR across sweep of ±2 T.

bility) with cooling that is reported for simple magnetic materials. A similar trend can be seen in the longitudinal magnetoresistance response in a perpendicular field as shown in Fig. 2b, with a spike in the same temperature range clearly shown in the inset. Our measured magnetoresistance values are similar in magnitude to those reported in past studies.[24,25]

The presence of a competing ferromagnetic/antiferromagnetic order explains these results. While many previous

studies on FGT samples of varying thicknesses report simple hysteresis loops that vary monotonically with temperature, others have reported similar trends in not only the Hall response but also in the anomalous Nernst response of the samples.[26–29] Variations in FGT's behavior across studies can potentially be explained by different sample thicknesses and growth conditions for the used crystals. As the temperature falls, an antiferromagnetic interaction between adjacent layers forms and grows stronger. This interaction is explained as the antiferromagnetic coupling between two ferromagnetic layers, similar to the interlayer interaction in few layer CrI_3.[17,30] Though antiferromagnetic behavior is predicted to emerge in FGT at around 150 K, based off our results it does not become strong enough to reduce the out-of-plane response until the temperature is lowered further to 120 K. The maximum response at this temperature agrees very well with measurements in ref. 17 conducted using SQUID magnetometry on mm-sized crystals.

Next, we measure the Hall response while rotating the sample in an applied magnetic field. In ferromagnets, changing the applied field direction away from the sample normal will often result in a planar Hall effect (PHE) signal. This contribution is distinct from the normal and anomalous Hall effects caused by an out of plane field and is linked to anisotropic magnetoresistance (AMR) in a material.[31] The PHE signal is maximized when the applied current makes a 45 degree angle with the magnetization direction and vanishes when the sample magnetization is parallel or perpendicular to the current.[32] AMR measurements on one of our samples did show a pronounced anisotropy emerging at lower temperatures (see Fig. S6†), with the largest magnetoresistance (MR) emerging with a field applied nearly in plane at 100 K. The PHE is often reported as producing a symmetric curve due to the nature of the AMR. Here however, we consistently measure strong anti-symmetric hysteresis loops at low temperature similar to the AHE when the applied field is rotated in-plane. Notably, in-plane measurements produce a strong, non-sinusoidal signal at lower temperatures and fields as shown in Fig. 3a and b. The curves also bear distinctive anti-symmetric humps, a commonly cited characteristic of the topological Hall effect (THE) caused by the presence of skyrmions. These results are very similar to those reported in other literature studying macroscopic FGT crystals, which named the phenomenon the planar topological Hall effect (PTHE) and attributed it to skyrmion formation.[5] Considering this effect, the total Hall signal can be expressed as $R_{xy} = R_0H_Z + R_sM_z + R_{PTHE}$. More recent work has directly imaged skyrmions in FGT/h-BN heterostructures similar to those used in our study, lending

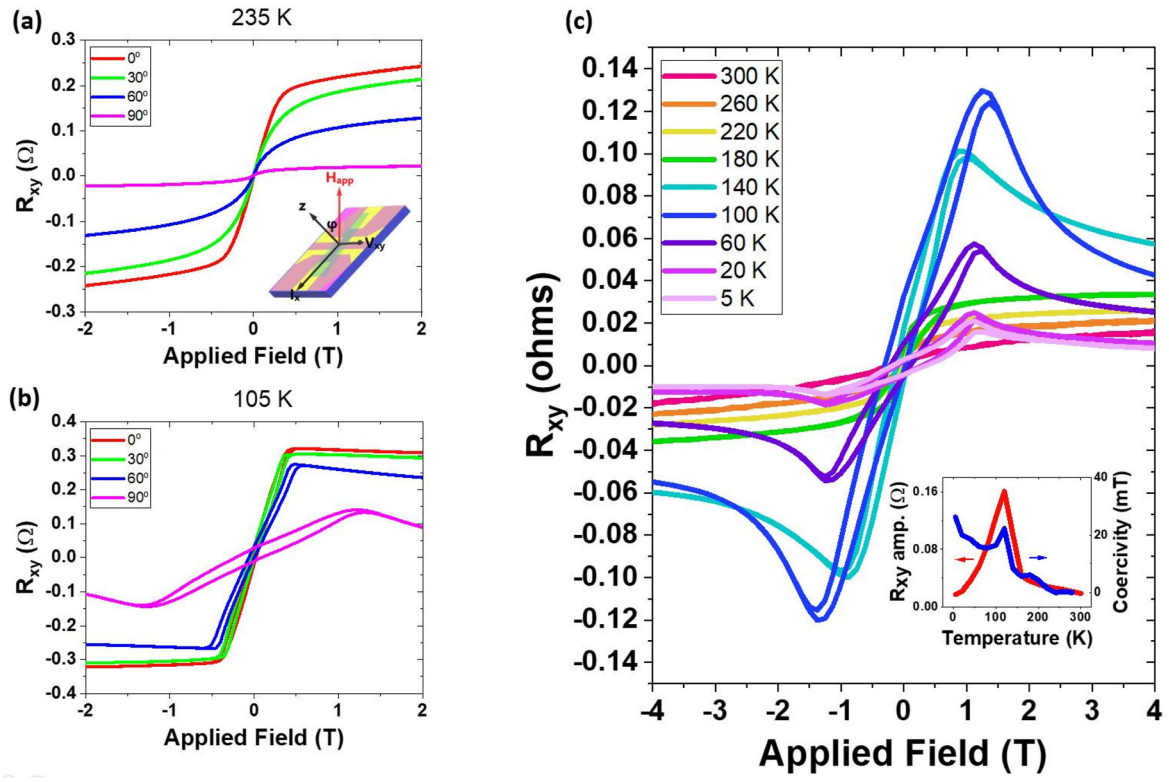

Fig. 3 In-plane Hall resistance in FGT samples. (a) and (b) Hysteresis loops measured at four angles at 235 K and 105 K, respectively. The THE signal becomes strong beneath 150 K, aligning with the emergence of the antiferromagnetic phase in FGT. Inset: schematic showing sample rotation in the applied field. See Fig. S8† for additional rotation-dependent data. (c) Hall resistance of Fe_3GeTe_2 at various temperatures for applied field parallel to the sample plane (φ = 90 deg). Inset: maximum Hall signal and coercivity *vs.* temperature. Due to small irregularities in sample mounting and rotation, alignment of the applied field with respect to the current direction may have a slight error.

credibility to this claim.[33] Importantly however, the samples in ref. 33 were fabricated under ambient conditions and thus have significant oxidation on the top and bottom of the FGT flake. These oxide interfaces are claimed to be the source of the Dzyaloshinskii–Moriya interaction (DMI) that gives rise to skyrmion formation. Our samples were exfoliated in a glovebox where the risk of significant oxidation is small, and they do not exhibit other features like tails in the hysteresis loop that suggest oxidized FGT (see Fig. S7†). Signals similar in shape to the THE not caused by skyrmions can arise in inhomogeneous systems, however this is unlikely here given the uniformity of exfoliated flakes.[34] Other work using both cryogenic magnetic force microscopy (MFM) and micromagnetic simulations however suggests that the DMI could be intrinsic to FGT without an oxide layer, arising from the broken inversion symmetry in individual FGT layers.[35] Assuming negligible oxidation in our samples, this explains the strong PTHE signal that was observed. Ultimately, however, more work is needed to pin down the precise origin of the DMI in FGT.

Despite the uncertainty of the planar topological Hall signal's origin in our samples, we can nonetheless see that it follows a trend very similar to that of the AHE and MR signals in the sample. Just like the out-of-plane measurements, the in-plane Hall signal rapidly peaks at 120 K before being suppressed at lower temperatures as is clearly seen in Fig. 3c. Assuming the observed signal is indeed the PTHE, this shows that skyrmion density is highest when the ferromagnetic phase is strongest. The results can again be qualitatively explained by returning to the intuitive picture of interlayer coupling giving rise to an out-of-plane antiferromagnetic phase. As the interlayer interaction increases, complex spin textures (including skyrmions) can no longer be stabilized and thus reduces the PTHE signal with decreasing temperature. In this way, temperature can be used to precisely control skyrmion density across different magnetic phases.

Lastly, we use the AHE to investigate the effects of cooling the sample in the presence of a magnetic field. Another strong signature of antiferromagnetic behavior in FGT comes from its field-cooling response.[17] Similarly to how field-cooling can be used to control systems with an EB present, field-cooling in a mixed phase system will affect susceptibility at lower temperatures. This can intuitively be thought of as the cooling field "locking" the antiferromagnetic-coupled spins into favorable orientations. This behavior is similar to so-called spin glasses, which mixed phase systems have been known to resemble.[36] Unlike the case of EB, the field cooling response will be nearly symmetric instead of anti-symmetric. Field-cooling measurements on our FGT samples were conducted by lowering the temperature from 300 K down to 5 K in the presence of a ±8 T field. Hysteresis loops were then measured at increasing temperatures as shown in Fig. 4a–c. These results clearly show a nearly matching field-cooling response, with the divergence between field-cooled (FC) and zero-field-cooled (ZFC) curves decreasing with increasing temperature as shown in Fig. 4d.

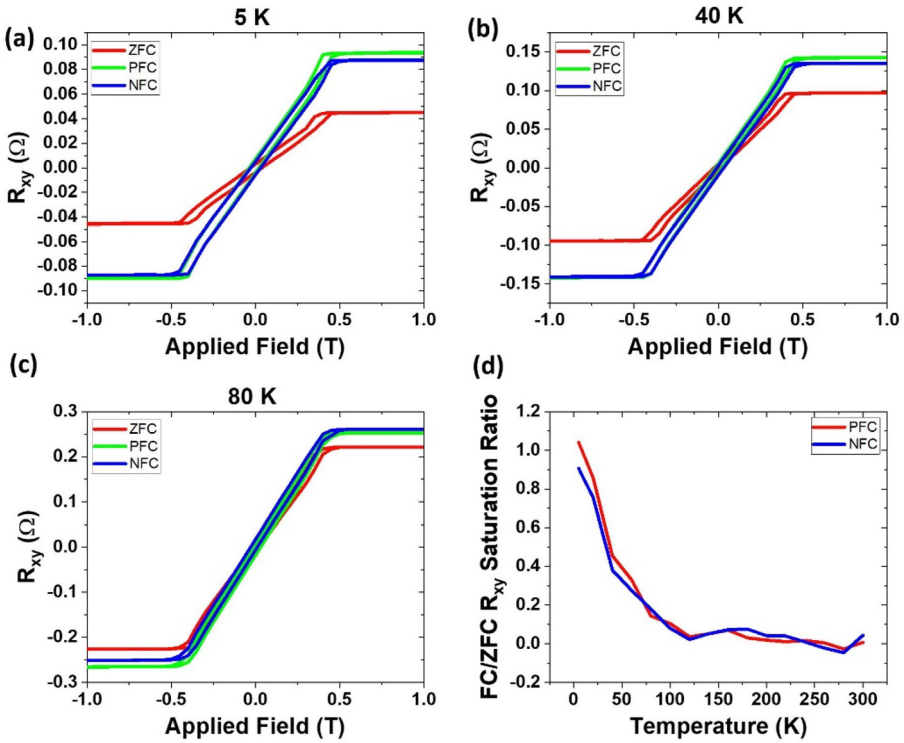

Fig. 4 Field cooling response of FGT sample. (a–c) Comparison of zero-field-cooled (ZFC), positive-field-cooled (PFC), and negative-field-cooled (NFC) Hall resistances at 5 K, 40 K, and 80 K respectively. See Fig. S9† for additional field-cooling data. (d) Ratio of ZFC to FC saturation Hall resistance as a function of temperature.

Both positive field cooling (PFC) and negative field cooling (NFC) increased the susceptibility compared to the zero-field cooled case, consistent with the presence of an antiferromagnetic phase. Measurements in our samples did not reveal a training effect, *i.e.*, repeated measurements at the same temperature did not change the shape of the hysteresis loop. This trend likely reflects the high energy cost of opposing the FC configuration which weakens at high temperature, thus reducing the divergence.

Conclusion

In summary, we have employed simple magneto-transport measurements to gain insight into the complex magnetic phase transitions of Fe_3GeTe_2. We observed a unique temperature dependence in the out-of-plane AHE and MR response that signifies changing dominance between ferromagnetic and antiferromagnetic phases in the samples. By rotating the applied field into the sample plane, we can observe similar trends in the planar topological Hall response. Finally, the use of the AHE to probe a field-cooling divergence in the sample unveils a spin glass like behavior consistent with a mixed phase system. Our results show that even simple transport measurements can be used to identify novel properties in vdW magnets. The unique behavior we have observed with these measurements makes FGT a promising material platform for investigating emerging physical phenomena and creating novel magnetic and spintronic devices.

Author contributions

S.T.C. designed and fabricated the FGT devices and carried out the transport measurements; S.T.C. and J.S. did atomic force microscopy measurements on the fabricated devices; H.L. completed EDS measurements on the bulk crystals. K.X. performed the initial transport study on FGT; P.F.F. provided training/insight for the flake transfer technique; W.Z. supervised the project; S.T.C. and W.Z. wrote the manuscript; and all authors gave their insight into the results.

Conflicts of interest

No conflicts to declare.

Acknowledgements

The authors would like to acknowledge the support from the Semiconductor Research Corporation (SRC) under grant SRC 2021-LM-3042, the University of Illinois at Urbana-Champaign under the Strategic Research Initiatives (SRI) program, and facilities within the Holonyak Micro/Nanotechnology Laboratory that made this work possible. The authors also acknowledge the use of facilities and instrumentation supported by NSF through the University of Illinois Materials Research Science and Engineering Center DMR-1720633 P. F. F and A. M. v. d. Z acknowledge support by NSF-CAREER Award number CMMI-184673.

References

1 X. Jiang, Q. Liu, J. Xing, N. Liu, Y. Guo, Z. Liu and J. Zhao, *Appl. Phys. Rev.*, 2021, **8**, 1–69.
2 C. Gong and X. Zhang, *Science*, 2019, **363**, eaav4450.
3 Y. Khan, S. M. Obaidulla, M. R. Habib, A. Gayen, T. Liang, X. Wang and M. Xu, *Nano Today*, 2020, **34**, 100902–100902.
4 Y. Wu, S. Zhang, J. Zhang, W. Wang, Y. L. Zhu, J. Hu, G. Yin, K. Wong, C. Fang, C. Wan, X. Han, Q. Shao, T. Taniguchi, K. Watanabe, J. Zang, Z. Mao, X. Zhang and K. L. Wang, *Nat. Commun.*, 2020, **11**, 3–8.
5 Y. You, Y. Gong, H. Li, Z. Li, M. Zhu, J. Tang, E. Liu, Y. Yao, G. Xu, F. Xu and W. Wang, *Phys. Rev. B: Condens. Matter Mater. Phys.*, 2019, **100**, 134441.
6 Z. Fei, B. Huang, P. Malinowski, W. Wang, T. Song, J. Sanchez, W. Yao, D. Xiao, X. Zhu, A. F. May, W. Wu, D. H. Cobden, J. H. Chu and X. Xu, *Nat. Mater.*, 2018, **17**, 778–782.
7 B. Huang, G. Clark, E. Navarro-Moratalla, D. R. Klein, R. Cheng, K. L. Seyler, D. Zhong, E. Schmidgall, M. A. McGuire, D. H. Cobden, W. Yao, D. Xiao, P. Jarillo-Herrero and X. Xu, *Nature*, 2017, **546**, 270–273.
8 C. Gong, L. Li, Z. Li, H. Ji, A. Stern, Y. Xia, T. Cao, W. Bao, C. Wang, Y. Wang, Z. Q. Qiu, R. J. Cava, S. G. Louie, J. Xia and X. Zhang, *Nature*, 2017, **546**, 265–269.
9 R. Roemer, C. Liu and K. Zou, *npj 2D Mater. Appl.*, 2020, **4**, 33.
10 Z. Wang, D. Sapkota, T. Taniguchi, K. Watanabe, D. Mandrus and A. F. Morpurgo, *Nano Lett.*, 2018, **18**, 4303–4308.
11 X. Wang, J. Tang, X. Xia, C. He, J. Zhang, Y. Liu, C. Wan, C. Fang, C. Guo, W. Yang, Y. Guang, X. Zhang, H. Xu, J. Wei, M. Liao, X. Lu, J. Feng, X. Li, Y. Peng, H. Wei, R. Yang, D. Shi, X. Zhang, Z. Han, Z. Zhang, G. Zhang, G. Yu and X. Han, *Sci. Adv.*, 2019, **5**, eaaw8904.
12 M. Alghamdi, M. Lohmann, J. Li, P. R. Jothi, Q. Shao, M. Aldosary, T. Su, B. P. T. Fokwa and J. Shi, *Nano Lett.*, 2019, **19**, 4400–4405.
13 Y. Zhang, H. Xu, C. Yi, X. Wang, Y. Huang, J. Tang, J. Jiang, C. He, M. Zhao, T. Ma, J. Dong, C. Guo, J. Feng, C. Wan, H. Wei, H. Du, Y. Shi, G. Yu, G. Zhang and X. Han, *Appl. Phys. Lett.*, 2021, **118**, 262406.
14 D. Kim, S. Park, J. Lee, J. Yoon, S. Joo, T. Kim, K. J. Min, S. Y. Park, C. Kim, K. W. Moon, C. Lee, J. Hong and C. Hwang, *Nanotechnology*, 2019, **30**, 245701.
15 J. Nogués and I. K. Schuller, *J. Magn. Magn. Mater.*, 1999, **192**, 203–232.
16 H. K. Gweon, S. Y. Lee, H. Y. Kwon, J. Jeong, H. J. Chang, K. W. Kim, Z. Q. Qiu, H. Ryu, C. Jang and J. W. Choi, *Nano Lett.*, 2021, **21**, 1672–1678.

17 J. Yi, H. Zhuang, Q. Zou, Z. Wu, G. Cao, S. Tang, S. A. Calder, P. R. C. Kent, D. Mandrus and Z. Gai, *2D Mater.*, 2017, **4**, 011005.
18 L. Thiel, Z. Wang, M. A. Tschudin, D. Rohner, I. Gutiérrez-Lezama, N. Ubrig, M. Gibertini, E. Giannini, A. F. Morpurgo and P. Maletinsky, *Science*, 2019, **364**, 973–976.
19 D. G. Purdie, N. M. Pugno, T. Taniguchi, K. Watanabe, A. C. Ferrari and A. Lombardo, *Nat. Commun.*, 2018, **9**, 5387.
20 H. Zhang, R. Chen, K. Zhai, X. Chen, L. Caretta, X. Huang, R. V. Chopdekar, J. Cao, J. Sun, J. Yao, R. Birgeneau and R. Ramesh, *Phys. Rev. B*, 2020, **102**, 064417.
21 N. Nagaosa, J. Sinova, S. Onoda, A. H. Macdonald and N. P. Ong, *Rev. Mod. Phys.*, 2010, **82**, 1539.
22 Y. Deng, Y. Yu, Y. Song, J. Zhang, N. Z. Wang, Z. Sun, Y. Yi, Y. Z. Wu, S. Wu, J. Zhu, J. Wang, X. H. Chen and Y. Zhang, *Nature*, 2018, **563**, 94–99.
23 C. Tan, J. Lee, S. G. Jung, T. Park, S. Albarakati, J. Partridge, M. R. Field, D. G. McCulloch, L. Wang and C. Lee, *Nat. Commun.*, 2018, **9**, 1554.
24 J. Ke, M. Yang, W. Xia, H. Zhu, C. Liu, R. Chen, C. Dong, W. Liu, M. Shi, Y. Guo and J. Wang, *J. Phys.: Condens. Matter*, 2020, **32**, 405805.
25 X. Zeng, G. Ye, S. Huang, L. Zhang, H. Xu, Y. Liu, H. Kuang, B. Ma, J. Luo, X. Lu and X. Wang, *J. Phys.: Condens. Matter*, 2022, **34**, 345701.
26 C. Fang, C. H. Wan, C. Y. Guo, C. Feng, X. Wang, Y. W. Xing, M. K. Zhao, J. Dong, G. Q. Yu, Y. G. Zhao and X. F. Han, *Appl. Phys. Lett.*, 2019, **115**, 212402.
27 J. Xu, W. A. Phelan and C. L. Chien, *Nano Lett.*, 2019, **19**, 8250–8254.
28 Y. Wang, C. Xian, J. Wang, B. Liu, L. Ling, L. Zhang, L. Cao, Z. Qu and Y. Xiong, *Phys. Rev. B*, 2017, **96**, 134428.
29 P. R. Sharma, T. W. Kim and H. Noh, *Mater. Chem. Phys.*, 2023, **302**, 127738.
30 S. Jiang, L. Li, Z. Wang, K. F. Mak and J. Shan, *Nat. Nanotechnol.*, 2018, **13**, 549–553.
31 T. Li, L. Zhang and X. Hong, *J. Vac. Sci. Technol., A*, 2022, **40**, 010807.
32 A. Elzwawy, H. Pişkin, N. Akdoğan, M. Volmer, G. Reiss, L. Marnitz, A. Moskaltsova, O. Gurel and J.-M. Schmalhorst, *J. Phys. D: Appl. Phys.*, 2021, **54**, 353002.
33 T.-E. Park, L. Peng, J. Liang, A. Hallal, F. S. Yasin, X. Zhang, K. M. Song, S. J. Kim, K. Kim, M. Weigand, G. Schütz, S. Finizio, J. Raabe, K. Garcia, J. Xia, Y. Zhou, M. Ezawa, X. Liu, J. Chang, H. C. Koo, Y. D. Kim, M. Chshiev, A. Fert, H. Yang, X. Yu and S. Woo, *Phys. Rev. B*, 2021, **103**, 104410.
34 A. Gerber, *Phys. Rev. B*, 2018, **98**, 214440.
35 M. J. Meijer, J. Lucassen, R. A. Duine, H. J. M. Swagten, B. Koopmans, R. Lavrijsen and M. H. D. Guimaraes, *Nano Lett.*, 2020, **20**, 8563–8568.
36 A. Bhattacharyya, S. Giri and S. Majumdar, *Phys. Rev. B: Condens. Matter Mater. Phys.*, 2011, **83**, 134427.